A New Coupled Electrodynamic T – A and Thermal Model for the Critical Current Characterization of High-Temperature Superconducting Tapes and Cables

IEEE Access
Multidisciplinary | Rapid Review | Open Access Journal

Received 28 August 2023, accepted 24 September 2023, date of publication 2 October 2023, date of current version 5 October 2023.

Digital Object Identifier 10.1109/ACCESS.2023.3321194

RESEARCH ARTICLE

A New Coupled Electrodynamic T − A and Thermal Model for the Critical Current Characterization of High-Temperature Superconducting Tapes and Cables

SOFIA VIARENGO[1,2], (Graduate Student Member, IEEE), LUCAS BROUWER[2], PAOLO FERRACIN[2], (Senior Member, IEEE), FABIO FRESCHI[1,3], (Senior Member, IEEE), NICOLO' RIVA[4], LAURA SAVOLDI[1], (Member, IEEE), AND XIAORONG WANG[2], (Senior Member, IEEE)

[1]Dipartimento Energia "Galileo Ferraris," Politecnico di Torino, 10129 Turin, Italy
[2]Lawrence Berkeley National Laboratory, Berkeley, CA 94720, USA
[3]School of Information Technology and Electrical Engineering, University of Queensland, Brisbane, Qld, 4072, Australia
[4]Plasma Science and Fusion Center, Massachusetts Institute of Technology, Cambridge, MA 02138, USA

Corresponding author: Sofia Viarengo (sofia.viarengo@polito.it)

This work was supported in part by Politecnico di Torino through the U.S. Magnet Development Program; and in part by the U.S.—Japan High Energy Physics Collaboration from the U.S. Department of Energy, the Office of the High Energy Physics.

ABSTRACT Future collider accelerators will rely on high-temperature superconductors reaching high field up to 20 T and above. Among the existing high-temperature superconducting materials, the Rare-earth Barium Copper Oxide (ReBCO) tapes arranged according to the Conductor-on-Round-Core (CORC®) concept could be a viable solution to wound accelerator magnets such as Cosine Canted Theta (CCT) magnets. Dedicated experimental characterization of the critical current to quantify the degradation due to the winding process and operating conditions should proceed in parallel to the development of numerical models capable to reproduce and, in perspective, predict the cable performance. This paper presents the development of a new multi-physics model for a CORC® wound with ReBCO tapes together with its validation. The $T - A$ formulation has been used leveraging the high aspect ratio of tapes, suitably coupled with a conduction thermal model which for the first time properly accounts for the cable convective cooling. The model developed in this work can accurately simulate the thermal, electric and magnetic behaviors and the current sharing among tapes by using a set of self-consistent boundary conditions adopted for the first time in this kind of simulations. The model is verified and benchmarked against other well-established formulations on a set of test cases. The comparison of the computed $V - I$ characteristic of the straight cable to available experimental data shows that the main physics features of the cable are well captured by the model, including performance degradation due to cable tapering at the terminations.

INDEX TERMS Numerical models, CORC® cables, critical current, multiphysics model, high-temperature superconductors, hybrid formulation.

I. INTRODUCTION

The next target for future colliders is reaching 20 T level field. One of the main challenges of the high field superconductor magnet is withstanding the Lorentz forces generated within the magnet. Within this framework, the Canted-Cosine Theta (CCT) magnet concept, proposed in 1970 [1], turns out to be particularly promising for strain-sensitive superconductors (SC), such as Low-Temperature superconductors (LTS) Nb_3Sn [2], and the High-Temperature Superconductors (HTS) Bi2212 [3] and Rare-earth Barium Copper Oxide (ReBCO) [4]. The CCT is based on a cable wound in

The associate editor coordinating the review of this manuscript and approving it for publication was Su Yan.

superposed layers of oppositely tilted solenoids such that the current distribution generates a pure harmonic field: in this configuration, the transverse field components will sum up, and the solenoidal will cancel out [5]. Within a single layer, the cable, assembled with standard conductors or SC wires or tapes, is contained within the grooves of a mandrel, avoiding the summation of electromagnetic forces [5]. Among the SC materials, the HTS ones constitute the most viable option towards the development of high field magnets satisfying the requirements of high operating currents, high current densities, and compact coil layouts [6], [7]. ReBCO superconductors represent one of the most promising alternative among HTS for the high critical current density and high critical temperature [8]. The capability of carrying much higher electrical current with respect to the LTS, guaranteeing at the same time a higher thermal stability, since the large difference between the critical temperature and the operational one (temperature margin), results convenient for high deposition and fast-ramping applications [9]. Moreover, the high irreversible field [10] of such conductors at low temperature, from 4.2 K to 20 K, allows them to generate dipole magnets up to 20 T and above, an impossible target for the LTS counterparts [4]. The strength of the Hastelloy layer present in ReBCO tapes enhanced their mechanical properties, which led toward the development of the Conductor-on-Round-Core (CORC®) design. The concept of CORC® cable was introduced in 2009 [11]: composed of several layers of HTS tapes helically wounded on a copper core with opposite winding direction for each layer, see Fig. 1b). That kind of cabling guarantees a high isotropic flexibility and mechanical strength [12], and reduction of AC losses [13], [14]. The core diameter is typically in the order of few millimeters and the winding angle is around 40 degrees. Nonetheless, such cables are subjected to degradation due to winding process and operating conditions. The mechanical strain can significantly degrade the CORC® performances [15], [16]. Mechanical analysis using finite element is particularly interesting for the prediction of the cable behavior [17], [18], [19], [20], [21], [22]. Another crucial aspects for the CORC® is the proper computation of the current distribution among tapes and the possible re-distribution due to external disturbance. Some simplified approaches simulate the current distribution on CORC® by an equivalent network model [23] or represent the 2D cross-section of cables where the helical structure is neglected [24], [25], [26], [27]. However, due to the peculiar geometry, those simplifications do not allow to properly reproduce the actual cable behavior and the accurate evaluation of losses, which mostly occur on CORC® edges [28], [29]. Therefore, 3D models are widely used especially focus on AC losses evaluation and magnetization. The well-known H-formulation is currently applied in such models [30], [31], [32], [33], [34] and it is usually considered as reference to verify other formulations [24], [26]. Recently, taking advantage of the high ReBCO aspect ratio, the hybrid $T - A$ formulation (firstly introduced in [35]), based on thin shell approximation of the conductive tape, is gaining interest in view of the saving in terms of computational time [24], [26], [29], [36], [37], [38]. While macroscopical quantities (i.e., magnetization and AC losses) can be properly calculated assuming an infinitely thin SC films, the local distribution of current density in AC cannot reliably computed inside the SC tape [34]. The method currently used to impose a transport current in the $T - A$ formulation doesn't guarantee any self-consistent current distribution (or redistribution) among tapes. In [39] an equivalent circuit model, applied also in [38], is proposed to compute the current redistribution during a quench, depending on the equivalent resistance of each tape and on self and mutual inductance. The model is coupled with the T formulation: the resistance is evaluated in the T module and the electric network gives back the current distribution. This procedure requires the implementation and the coupling with a third lumped circuit module, creating additional issues on the convergence and stability of the solution. In [26] a Neumann boundary condition, which allows a coupling effect between the T and the A, is presented. It is demonstrated in the paper that the current redistribution is affected by **A** through the electric field **E** across the boundary and **B** inside the tape. The condition is given in a weak form, and it allows a non-uniform redistribution of the current in the cable. However, this condition increases the complexity of the problem along with the risk that the current is not conserved.

In this paper, a fully 3D CORC® multi-physics model, which for the first time guarantees a proper current redistribution among tapes and layers, is presented. A new boundary condition is proposed in the strong form: the redistribution of the current in the cable is guaranteed imposing, among two subsequent boundaries, the current vector potential **T** to be uniform and equal, see Section III-B1. The main novelty with respect to previous works is the model capability to compute and redistribute the current without any external circuital network, according to possible disturbance or defect on each tape (i.e., hot spot temperature or electromagnetic difference).

Thermal effects are strong drivers of the behavior of HTS cables, multiphysics models combining the $T-A$ formulation to a thermal model in thin shells are already available in literature [24], [39], aiming to simulate quench behavior. In those models, the heat source term is due to the Joule losses within the conducting domain and an external heat source, if any. No other heat sink takes into account the refrigeration with the coolant, by risking an underestimation of cable performances. An exact formulation based on the $T - A$ formulation with a proper consideration of the convection due to the refrigerant is still missing in literature.

Here, for the first time the $T - A$ formulation for electromagnetic module is suitable coupled to a heat transfer thin shells model, accounting also for the convective cooling of the cryogen, properly developed in COMSOL Multiphysics® [40]. The model relies on a multiscale approach starting

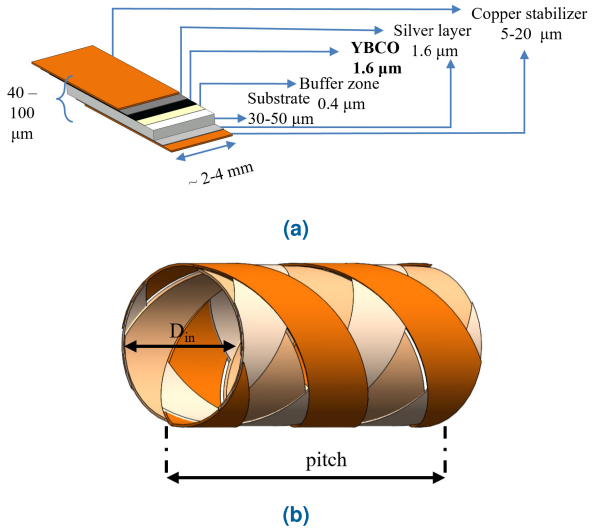

FIGURE 1. (a) YBCO tape cross section and tape layers' thicknesses. (b) Sketch of the CORC® cable investigated here (copper core not represented here).

from the homogenization of the tape properties that are then applied to the CORC® cable. The model has been verified and benchmarked against the well-know $H-$formulation, and it has been able to reproduce the $V-I$ characteristic curve and validated with respect experimental data obtained at Lawrence Berkeley National Laboratory (LBNL).

In Section II, we report the ReBCO tape geometry and properties characterization. Section III, discusses in detail the mathematical models used for the critical current calculation and the electromagnetic and thermal simulations, namely a 2D magnetostastic model for the calculation of the critical current value (i.e. for one point on the $V-I$) and two time-dependent models to simulated the entire $V-I$ curves based on the $T-A$ formulation. Additionally, we describe in detail boundary conditions related to the different cases. In Section IV, the verification and the benchmark against the $H-$formulation and experimental data are shown. Finally, Section V is devoted to the conclusions.

II. YBCO TAPES

Among ReBCO materials, the Yttrium Barium Copper Oxide (YBCO) coated conductor tapes are the ones considered in this study. They are characterized by a high critical temperature, of 93 K, and they are able to transport high current densities at very high fields. The YBCO tapes, such as those of SuperPower inc [41], are composed of different layers and characterized by a thickness of few micrometers (some common dimensions are reported in Fig. 1a). The superconductor layer is coated by a copper stabilizer, and a metal substrate, made of Hastelloy, is present as a mechanical support to axial and bending stresses. The thermo-physical properties of all materials are considered dependent on the residual resistivity ratio ($RRR \approx 40$ for SuperPower tapes [42]), which is an index of the purity of

TABLE 1. YBCO layer material properties at 77 K from [43].

Material	λ (W/m/K)	ρ (kg/m^3)	C_p (J/kg/K)	σ (S/m)
YBCO	5.914	6,390	88.69	Eq. (3)
Silver	530.4	10,630	161.4	3.17×10^8
Copper	431.2	8,960	218.1	3.47×10^8
Hastelloy	7.801	8,890	163.5	8.40×10^5
Homog.	204.1	8,936	185.2	Eq. (6)

the material defined as the ratio between the resistivity at room temperature and that at 0 K (for any material) or at the transition temperature (for SC), and temperature. The thermo-physical properties of the tape, taken from [43], have been homogenized on the tape cross section, and those at 77 K are summarized in Table 1. In detail, the homogenization has been obtained weighting the density ρ with the cross section, while the specific heat at constant pressure c_p with the mass. The thermal conductivity λ is strongly anisotropic: along the direction parallel to the tape surface, thermal resistances are arranged in parallel, whereas along the perpendicular direction, resistances are arranged in series. Therefore, the equivalent thermal conductivities λ_{eq} and $\lambda_\perp$ are properly evaluated and weighted on the cross section:

$$\lambda_{eq} = \frac{\sum_{i=1}^{N_l} \lambda_i A_i}{\sum_{i=1}^{N_l} A_i} \tag{1}$$

$$\frac{1}{\lambda_\perp} = \frac{\sum_{i=1}^{N_l} \frac{1}{\lambda_i} A_i}{\sum_{i=1}^{N_l} A_i} \tag{2}$$

where A is the cross section of the ith layer and N_l is the number of layers.

Regarding the electrical properties, the electrical conductivity σ of all but the YBCO layer, are temperature dependent, from [43], and the ones at 77 K are summarized in Table 1. For the SC layer, σ_{YBCO} is computed through the nonlinear power law:

$$\sigma_{YBCO} = \frac{J_c\left(B_\parallel, B_\perp, \theta\right)}{E_0}\left(\frac{|\mathbf{J}|}{J_c\left(B_\parallel, B_\perp, \theta\right)}\right)^{1-n} \tag{3}$$

where E_0 is the critical field (conventionally set to 1 μV/cm, n is the exponent of the power law, and $\mathbf{J}$ is the current density in the superconductor. The critical current density J_c characterization is based on Kim-like model [44], [45] and it is dependent on the magnetic flux densities parallel, $B_\parallel$, and normal, $B_\perp$, to the tape surface and on temperature θ:

$$J_c\left(B_\parallel, B_\perp, \theta\right) = \psi \frac{I_{c0}}{A_{sc}}\left(\frac{\theta_{c0}-\theta}{\theta_{c0}-\theta_0}\right)^\beta \frac{1}{\left[1+\frac{\sqrt{(kB_\parallel)^2+B_\perp^2}}{B_c}\right]^b} \tag{4}$$

where I_{c0} is the critical current at zero-field applied, A_{sc} is the SC cross section, θ_{c0} is the critical temperature at zero applied field, θ_0 is nominal operating temperature, θ is the actual tape temperature. β, k, B_c and b are fitting parameters that allow

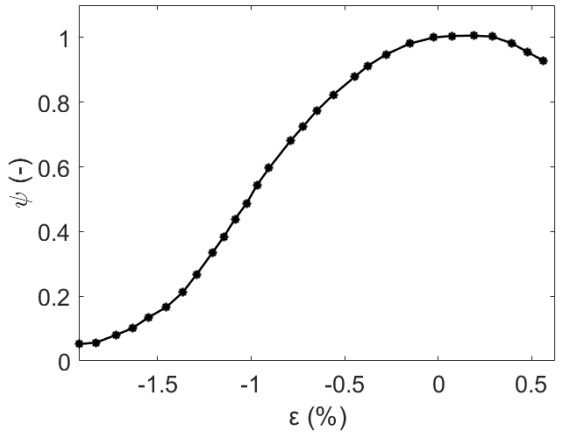

FIGURE 2. Critical current degradation ψ with respect to strain ε for YBCO tape in the midplane from [15].

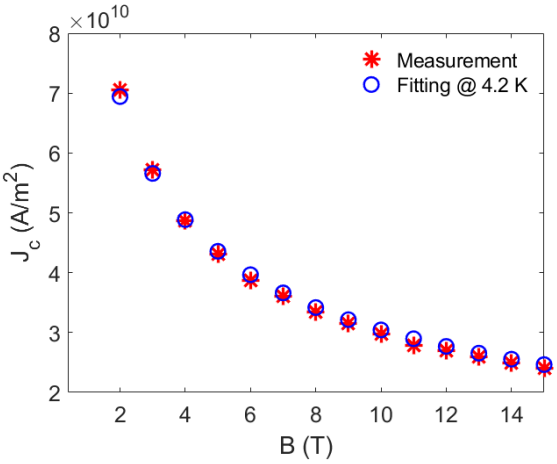

FIGURE 3. Critical current density fitted vs experimental data.

TABLE 2. J_c characterization: fitting parameters for a single tape.

Parameters	Value		Units
θ_0	4.2	77	K
I_{c0}	2197	85	A
$\theta_{c0-YBCO}$	93		K
β	1		–
k	0.275		–
B_c	100		mT
b	0.525	0.25	–
ψ	see Fig. 2		–

to weight the contributions due to θ, $B_\parallel$ and $B_\perp$. ψ represents the critical current density degradation expressed as I_c/I_{c0} due to the strain which the tape is subject to. Conservatively, the YBCO tape width has been considered uniformly under the maximum compression strain in % evaluated, from [15], as follows:

$$\varepsilon_{max} = \frac{-t_{sub}}{t_{sub} + d_{former} + 2t_{cu}} \tag{5}$$

where t_{sub} is the substrate thickness, d_{former} is the copper core diameter and t_{cu} is the copper layer thickness. The strain is evaluated on the mid plane of the tape. From [15], the degradation due to the winding is extrapolated from the graph in Fig. 2. All other parameters are reported in Table 2.

The scaling of the critical current density, evaluated as expressed in (4), has been computed by best-fitting the parameters β, k, B_c and b to the measurement data at LBNL on a 8 mm-long tape (more information can be found in [46]), see Fig. 3). The measurements have been carried out in self-field at 4.2 K and at 77 K and in different background fields at 4.2 K, from 0.4 T to 15 T imposed perpendicular to the tape surface [46]. Finally, the homogenization of the tape electrical properties has been achieved considering the electric parallel among layers, defining an equivalent electrical conductivity σ_{eq}, weighted on cross sections:

$$\sigma_{eq} = \frac{\sum_{i=1}^{N_l} \sigma_i A_i}{\sum_{i=1}^{N_l} A_i} \tag{6}$$

where σ_i is the electrical conductivity of the ith layer.

Note that the buffer zone has been neglected in the homogenization of tape materials, because the material is nonconducting.

III. NUMERICAL MODEL

In this section, we describe the numerical models used in this paper: a simple 2D magnetostastic model for the calculation of the single critical current values and electromagnetic-transient models $T - A$ formulation. The $H-$ formulation [30], [31] is not described in the paper for sake of brevity.

A. MAGNETOSTATIC 2D MODEL FOR THE OF A INFINITE NON-TWISTED TAPE/CABLE

The critical current of a 2D infinite non-twisted 3 layers CORC® is calculated according a modeling approach described in [47]. The model solves a magnetostatic problem (A-formulation) finding the distribution of the vector potential A such that inside the superconductor the current density is $J = J_c(B_\parallel, B_\perp)$ everywhere. The critical current of the 2D cross section cable is determined by integrating the critical current density distribution obtained from the model over the stack cross section.

B. MAGNETO-QUASISTATIC MODEL

Under the magneto quasi-static approximation, the $T - A$ formulation [35] for the tape electromagnetic model is based on the introduction of two potentials: the current vector potential **T** for the conducting shell domain, and the magnetic vector potential **A** for the whole domain. When the conductor is approximated as thin shell, the current only flows along the tangential direction of the tape and

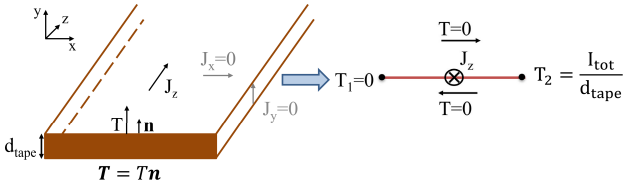

FIGURE 4. Sketch of thin approximation for T formulation and boundary condition in the case of transport current. T is always perpendicular to the tape surface, T_1 and T_2 are the values of T at the left and right edges, respectively, and d_{tape} is the tape thickness.

it is supposed to be uniform along the width, neglecting the component orthogonal to the surface. Therefore, $\mathbf{T}$ is considered perpendicular to the shell surface and the current density $\mathbf{J}$ can be evaluated as:

$$\mathbf{J} = \nabla \times \mathbf{T} = \nabla \times T\mathbf{n} \tag{7}$$

where T is a scalar variable and $\mathbf{n}$ is the unit vector orthogonal to the tape surface, see Fig. 4. The governing equation, based on Faraday's law is:

$$\nabla \times \left[\frac{1}{\sigma_{eq}} \nabla \times T\mathbf{n}\right] \cdot \mathbf{n} = -\frac{\partial \mathbf{B}}{\partial t} \cdot \mathbf{n} \tag{8}$$

$\mathbf{A}$ is defined over the entire computational domain, and the magnetic flux density $\mathbf{B}$ is computed as:

$$\mathbf{B} = \nabla \times \mathbf{A} \tag{9}$$

Coupled with Ampere's law, the governing equation is:

$$\nabla \times \left(\frac{1}{\mu} \nabla \times \mathbf{A}\right) = \mathbf{J} \tag{10}$$

where μ is the magnetic permeability. More theoretical foundation for the $T - A$ formulation can be found in [24], [26], [29], [35], [36], [37], and [38]. The model is fully coupled: the two variables $\mathbf{T}$ and $\mathbf{A}$ are solved simultaneously. $\mathbf{J}$ is the driver for the A formulation, while the variation of $\mathbf{B}$ with respect to time is the source in the T equation (8). The T formulation has been properly implemented for the condcuting domain in COMSOL Multiphysics® through *General Form Boundary PDE* module, while for the A formulation, the built-in *Magnetic Fields* module has been exploited using finite elements.

1) BOUNDARY CONDITIONS

In the T formulation, the transport current I on the tape is imposed through a Dirichlet boundary condition, obtained integrating the $\mathbf{J}$ over the tape cross-section $\mathbf{S}$ [35]:

$$I = \int \mathbf{J} \cdot d\mathbf{S} = \int (\nabla \times T\mathbf{n}) \cdot d\mathbf{S} = (T_1 - T_2)\, d_{tape} \tag{11}$$

where T_1 and T_2 are the value of T on the HTS edges and d_{tape} is the tape thickness, see Fig. 4.

In case of multiple tapes, to guarantee the correct current split among the tapes, the vector potential T is imposed to be 0 along the first boundary, equal to the total current I_{tot} along the last boundary, and to be uniform and equal among two subsequent boundaries, see Fig. 5 and in APPENDIX. The uniformity along the edge guarantees that no current would leak from that edge, while the equality is required to fulfill (11) including all tapes.

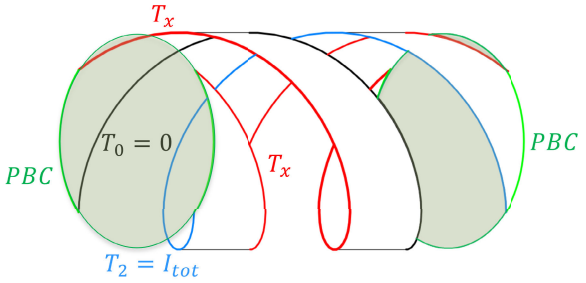

FIGURE 5. Sketch of the boundary conditions on 2 tapes CORC®: periodic boundary conditions (PBC) are highlighted in green, and in red the new boundary condition is presented. In the first boundary, T has been set equal to zero as a reference, and the total current is imposed in the last boundary (blue line).

TABLE 3. Liquid nitrogen properties at 77 K from NIST.

Parameters	Value	Units
β_f	0.013	1/K
λ_f	0.147	W/m/K
ρ_f	809.9	kg/m^3
$C_{p,f}$	2030	J/kg/K
ν_f	2.04	m^2/s
α_f	8.91×10^{-8}	m^2/s

When a CORC® cable is modelled, to exploit the minimum computational domain, just a pitch has been simulated and proper periodic boundary conditions are imposed, both in the SC and air domains, to avoid edge-effects, see Fig. 5.

In presence of an external magnetic field $\mathbf{B}_0$, it is applied as a boundary condition on the air domain: a suitable impressed magnetic vector potential $\mathbf{A}_0$, whose curl provides the three components of $\mathbf{B}_0$, (9), is imposed on the boundary edges of the computational domain.

C. THERMAL MODEL

The energy conservation law is solved only for the SC domain:

$$\rho_{eq} c_{eq} \frac{\partial \theta}{\partial t} = -\nabla \cdot \left(\lambda_{eq}(\theta) \nabla \theta\right) + \dot{q}(\theta) \tag{12}$$

where θ is the temperature, ρ_{eq} is the homogenized density, C_{eq} is the homogenized specific heat, λ_{eq} is the homogenized thermal conductivity along the parallel direction (see (1)), and finally $\dot{q}$ is the source term (see next sections for details). The solution has been obtained using the built-in *Heat Transfer in Shells* COMSOL module. The application of CORC® cables in CCT would be in a cryogen bath: the fluid is not simulated here, but the convective heat transfer is taken into account through an external heat sink.

1) SINGLE TAPE

For the single tape model, the source term is given by the sum of two contributions:

$$\dot{q}(\theta) = \dot{q}_j + \dot{q}_f(\theta) \tag{13}$$

where $\dot{q}_j$ is the dissipated power by Joule effect and $\dot{q}_f$ is the cooling power due to the liquid nitrogen bath. The Joule power is computed considering the equivalent conductivity:

$$\dot{q}_j = \frac{|J|^2}{\sigma_{eq}} \tag{14}$$

where J is the current flowing in the SC domain. The heat sink due to the refrigeration is computed as:

$$\dot{q}_f(\theta) = \frac{h_f A_{wet}(\theta_f - \theta)}{V_t} \tag{15}$$

where A_{wet} is the tape wetted area (equal to the tape surface), V_t is the tape volume, θ_f is the bath temperature, and θ is the actual tape temperature. The heat transfer coefficient h_f is evaluated starting from Nusselt number Nu, the tape characteristic length L_c and nitrogen thermal conductivity λ_f:

$$h_f = \frac{\lambda_f Nu}{L_c} \tag{16}$$

The Nusselt number has been computed through a proper correlation for horizontal plate in free convection for laminar flows from Rayleigh number [48]:

$$Nu = 0.54\, Ra^{\frac{1}{4}} \tag{17}$$

The Rayleigh number Ra is given as:

$$Ra = \frac{g\beta_f(\theta - \theta_\infty) L_c^3}{\nu_f \alpha_f} \tag{18}$$

where g is the gravity acceleration, β_f is the volumetric thermal expansion coefficient, ν_f is the dynamic viscosity, α_f is the thermal diffusivity, θ_∞ is the environment temperature (equal to the bath temperature), θ is the tape temperature, and L_c is the characteristic length of the geometry (defined as the ratio between the heat transfer area and the perimeter of the geometry). The pedix f is referred to the refrigerant fluid.

2) CORC® CABLE

For the CORC® model, the source term has one more contribution:

$$\dot{q} = \dot{q}_j + \dot{q}_f + \dot{q}_l \tag{19}$$

where $\dot{q}_l$ is the conductive contribution among adjacent layers computed as:

$$\dot{q}_l = \frac{\lambda_\perp}{\delta}(\bar{\theta}_i - \bar{\theta}_j)\frac{A_{contact}}{V_t} \tag{20}$$

where $\lambda_\perp$ is the homogenized transversal thermal conductivity (see Eq. (2)), δ and $A_{contact}$ are the distance and the contact area between two adjacent layers, respectively, $\bar{\theta}_i$ and $\bar{\theta}_i$ are mean temperature of the layers i and j (with $i \neq j$). The Joule effect and the cooling power are evaluated as reported in the previous section, but the Nusselt number has a different form: the cable has been approximated as a long horizontal cylinder and Nu is depending on the Rayleigh number Ra and in the Prandtl number Pr [48] as follows:

$$Nu = \left(0.6 + \frac{0.387\, Ra^{\frac{1}{6}}}{\left[1 + \left(\frac{0.559}{Pr}\right)^{\frac{9}{16}}\right]^{\frac{8}{27}}}\right)^2 \tag{21}$$

The model has is pretty flexible, and it has been recently used to model, for instance, twisted-stacked HTS cables [49].

TABLE 4. Test cases and set of simulations.

Model	Single tape	2-tape CORC®	6-tape CORC®
$T - A$ formulation	x	x	x
H formulation	-	x	-
2D magnetostatic	x	-	-
Measurements	x	-	x

D. ELEMENT ORDER

Regarding the element order of the utilized bases function for the finite element the discretization of the A-domain should always be one order higher than that of T-domain [50]. In [51] and [52] it is reported that, under sub-critical region, some oscillations can occur in the computed current density J, with first or second order Lagrange elements for both T and A. Therefore, all simulations have been carried out using first order linear element for the T formulation and second order quadratic element for the A formulation. Quadratic elements have been also used for the thermal module. The problem is fully coupled, therefore coupling effects and losses are automatically taken into account by the COMSOL.

IV. MODEL VERIFICATION AND VALIDATION

The model illustrated in Section III has been benchmarked following a step-by-step approach. First, a 3D model of single tape at 77 K has been verified and benchmarked against a magnetostatic model and measurements. The same model has been used for the prediction of the electric field-current ($E - I$) curves at different external magnetic fields, perpendicularly applied to the tape surface. Then, it has been extended to CORC® cables: a 2-tapes (1 layer) CORC® subject to the thermal perturbation and a 6-tapes CORC® (3 layers) for the replication of $V - I$ curve compared with experimental data. The set of tests cases is summarized in Table 4.

A. VERIFICATION AND BENCHMARK OF THE SINGLE TAPE T − A MODEL

This section is dedicated to test the model capability to deal with the strong non-linearity of the problem. A fully 3D model has been used for a straight 8 mm-long and 4 mm-wide tape [46], and validated with measurements. The problem has translational symmetry and can suitably be studied with a 2D model. The 3D model, necessary for more complex

TABLE 5. Tape thicknesses for single tape model.

Layer	Thickness	Units
YBCO	1.6	μm
Silver	1.6	μm
Copper	20	μm
Hastelloy	50	μm
Tape	95.2	μm

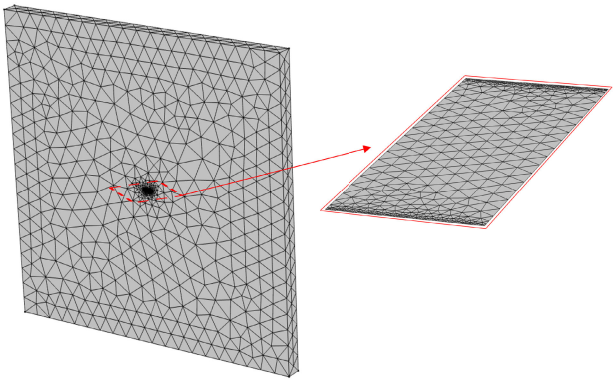

FIGURE 6. Illustration of the 3D meshed air and tape domains used for the solution in COMSOL for the tape model solved by the $T - A$ formulation.

geometries like the CORC® configuration, is here used to verify the capability of reproducing the 2D results. The model has been first verified through a grid independence, and then I_c values have been compared to the 2D magnetostatic model. Table 5 reports the geometric parameter of the SC tape.

1) EXPERIMENTAL SET-UP

A YBCO tape has been tested in the bath a liquid helium at 4.2 K and in a liquid nitrogen bath at 77 K. The sample has been soldered to a printed circuit board and the voltage has been measured using voltage taps at a distance of 5 mm (more details in [46]).

2) MESHES

The mesh of the 2D air domain, is triangular and a distribution of 100 nodes is guaranteed in the tape for the magnetostatic model. The mesh counts 8200 elements.

The 3D mesh for the $T - A$ model tape counts 10100 tetrahedral elements for the air domain and 2700 triangles for the tape, see Fig. 6. The $T - A$ model has been preliminary verified through a grid convergence analysis. The node distribution on the tape domain has been parametrically refined from 10 nodes till 250, and the I_c and the temperature gradient $\Delta\theta$ has been observed till reaching a plateau trend. In Fig. 7, the I_c and the $\Delta\theta$ variations are reported as a function of the nodes on the tape edge. For both quantity, the selected grid is proved to provide values already in the asymptotic regime.

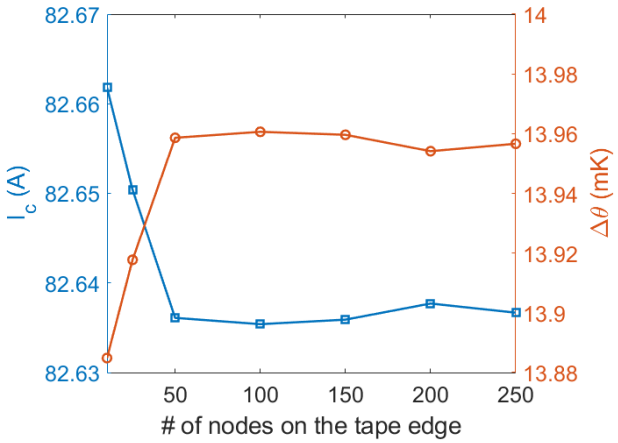

FIGURE 7. Blue line with square marker: tape critical current I_c as a function of the number of nodes along the tape edge. Red line with circled marker: tape gradient temperature $\Delta\theta$ as a function of the number of nodes along the tape edge at the critical state.

3) RESULTS

The critical current value calculated with the magnetostatic model at 77 K, self-field, was $I_{c,2D} = 82.3$ A and is represented by a yellow-filled green-circled marker in Fig. 8a. This value is very close to the nominal $I_c = 85$ A at 0-magnetic field as the self-magnetic field generated by a single tape is in the order of mT. The I_c computed from $T - A$ model is ∼82.6 A, with a relative error of 0.36% with respect the magnetostatic model. The relative error is about 1.35% compared to the measured value of ∼83.76 A. The calibrated n-value is 22, with an error of 13% with respect to the value extrapolated from experimental data, ∼25. The $V - I$ curves are reported in Fig. 8a.

The temperature increases about 20 mK when the current reaches the I_c, and it can rise of about 80 mK at 1.07 I_c∼90 A (when the tape transits to the normal state). In Fig. 8b, joule losses and the cooling power required for the liquid nitrogen are reported: the trend is in a very good agreement with the $V - I$ curve.

Additionally, simulations of the I_c value with an applied external field varying form 0.5 T to 5 T were performed and reported in Table 6. The magnetic field is uniform and imposed transversally to the tape surface. In Fig. 9, we plot the prediction of $E - I$ curves ($T - A$ formulation 3D) as well as the critical current prediction (magnetostatic 2D) for different fields applied perpendicularly to the flat-wide face of the tape. Note that the $n-$value was kept at a constant value $n = 22$. The model results are in good agreement (at I_c) and, as expected, the I_c experiences a strong field dependence with an increasing amplitude of the field. At the maximum applied magnetic field (5 T, likely the maximum operating point for CCT working at 77 K with CORC®), the I_c reduces by 40%. No higher fields were explored since the irreversible field of ReBCO at 77 K is 8 T [10].

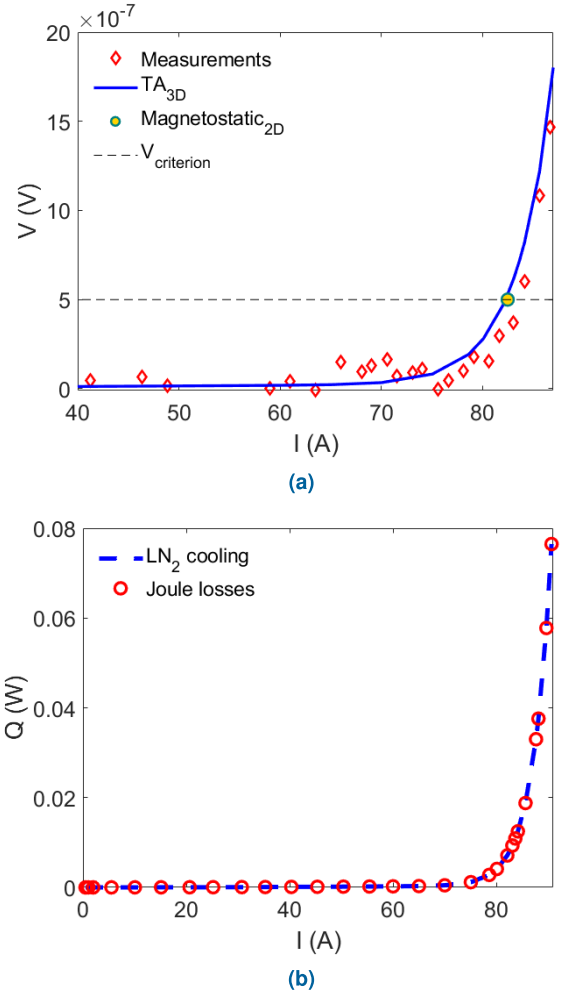

FIGURE 8. (a) Single tape $V - I$ curve, in self field at 77 K: experimental data (red square), 3D $T - A$ simulation (blue solid line), 2D magnetostatic model (yellow circle). (b) Joule losses (red dotted line) and required cooling power (blue dashed line) vs current.

TABLE 6. I_c value as function of the external perpendicular magnetic field.

Magnetic Field B (T)	Magneto-static model I_c (A)	$T - A$ formulation I_c (A)
0.5	53.9	54.0
1	46.5	46.0
1.5	42.4	42.0
2	39.5	39.5
2.5	37.5	37.8
3	35.8	35.8
5	31.7	31.3

B. BENCHMARK THE T – A MODEL OF A 2-TAPE CORC®

This section is dedicated to the demonstration that the current is able to properly redistribute among tapes, if any thermal perturbation suddenly happens. The $T - A$ formulation results are compared just with the H-formulation, since no experimental data are available. The CORC® geometry under study is constituted by 1 layer with 2 tapes, shown in

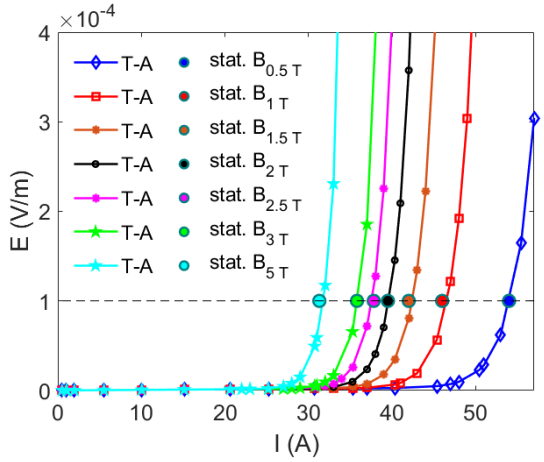

FIGURE 9. Prediction of computed $E - I$ curves for the single tape at different transverse imposed external field.

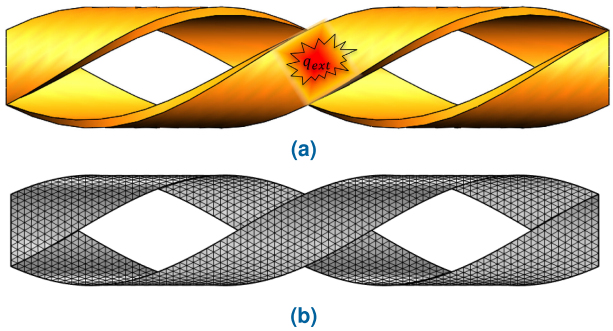

FIGURE 10. (a) Sketch of CORC® cable geometry used for case study 2. (b) Mesh used for the current case.

Fig. 10a: the tape geometrical data is reported in Table 5. The CORC® is characterized by a core diameter of 5.2 mm and a pitch of 30 mm. In one of the tape, a heat pulse is imposed, with a consequent rise in temperature and the current flows in the other two tapes. There is no thermal contact between the two tapes.

1) SIMULATION SET-UP

The current ramps-up in 0.1 s reaching a flat top of $I_{ext} = 85$ A (each tape experiences 0.5 I_{c0}). Heat is deposited at the center of one of the tapes via a gaussian pulse starting at 0.12 s and placed at the center of the tape over a length of 2 mm, see Fig. 10a. The volumetric heat source q_{ext} has been computed to increase the temperature of about 10 K. The heat releases a thermal energy of $E_{ext} = 45$ mJ, without taking into account of joule losses.

2) MESHES

In the $T - A$ model, the 3D air domain has been discretized with an unstructured tetrahedral mesh (about 53000 tetrahedral) and the 2D CORC® tape surfaces with unstructured triangular mesh (about 3800 triangles), see Fig. 10b. In the H model, the mesh counts for a total

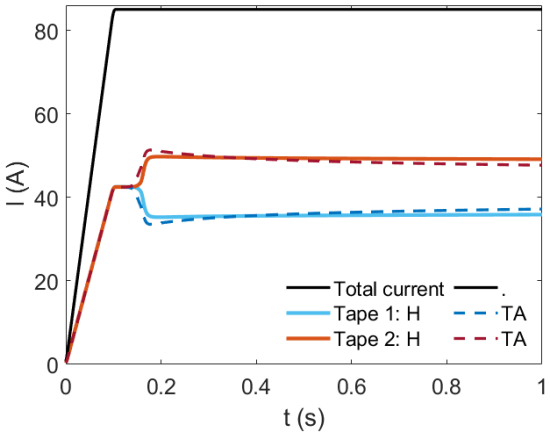

FIGURE 11. 2-tape CORC® current evolution: solid lines correspond to *H*-formulation results, dashed lines correspond to *T* – *A* formulation results.

number of elements of 66000: tapes have been meshed with a tetrahedral structured mesh counting for 3 element along the thickness and 60 element along the length. The air has been discretized with an unstructured tetrahedral mesh. The simulation ends at 1 s with a timestep $dt = 0.1$ ms, that it is refined during the heating time.

3) RESULTS

The current is ramped up on the 2-tape CORC® , and it is equally split among the two tapes, see Fig. 11. At 0.12 s, the external heat source is switched on, and the tape starts to rise in temperature, with a consequent resistivity increase, so that the current flows in the other tape. At 0.17 s, the peak temperature of ∼86.5 K, see Fig. 12b, so that the current is increasing in the second tape. In Fig. 13, current and temperature maps are reported at different time to show how the current redistributes.

In Fig. 11, transport currents flowing in the two tape computed from $T-A$ model are reported and compared with a $H-$formulation. When the heating is starting, the $T-A$ is in good agreement with the H-formulation, and the current in the second tape is rising with the same rate. At the peak, and the recovery is faster in the $T-A$-formulation than in the $H-$formulation, with a maximum error of 8%. In Fig. 12a the external power and the cooling are compared: they are in perfect agreement. From Fig. 12b, the maximum temperature reached of the heated tape is reported for both the volume and thin shell module: the maximum error between them is $< 0.1\%$.

The $T-A$ counts for about 346000 degrees of freedom (DoFs), while the $H-$formulation for about 193000 DoFs: the former has a total computational time of about 1 h and 45 min, the latter for of about 2 h and 30 min, showing an advantage in saving time.

C. 6-TAPE CORC® CABLE

Finally, the $T-A$ model has been validated with more complex geometry constituted by a 6-tape CORC® cable,

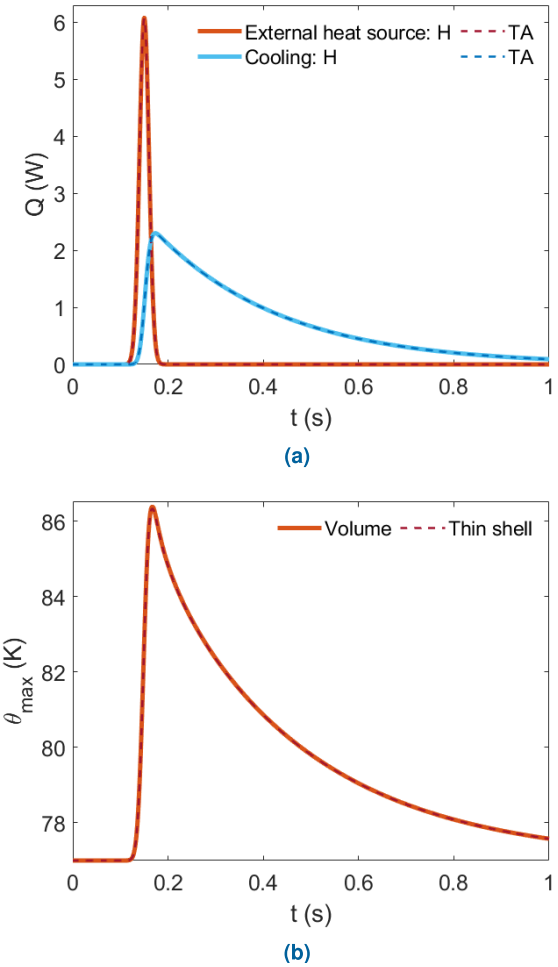

FIGURE 12. (a) External heat source in red, and computed cooling power in blue. Solid lines correspond to 3D model coupled with *H*-formulation, dashed lines correspond to thin shell model coupled with *T* – *A* formulation results. (b) Total Joule losses in 2-tapes CORC® : solid line is the volume model, the dashed line is the thin shell.

TABLE 7. 6-tape CORC® geometry parameters.

Parameters	Value	Units
YBCO thickness	1.6	μm
Silver thickness	1.6	μm
Copper thickness	5	μm
Hastelloy thickness	20	μm
Tape thickness	45.2	μm
Core diameter	2.76	mm
Cable pitch	5.7	mm
CORC® diameter within the termination	4.7	mm

operating at 77 K, test at the LBNL. The CORC® cable under study is composed of 3 layers with 2 tapes per layer, as shown in Fig. 1b, having a length of 0.5 m. Table 7 summarizes the main geometrical parameters of the CORC® under study.

1) EXPERIMENTAL SET-UP

The experimental setup is the same utilized for the CORC® cable manufactured for testing the Vacuum Pressure Impregnation (VPI) process [53]. From the cable

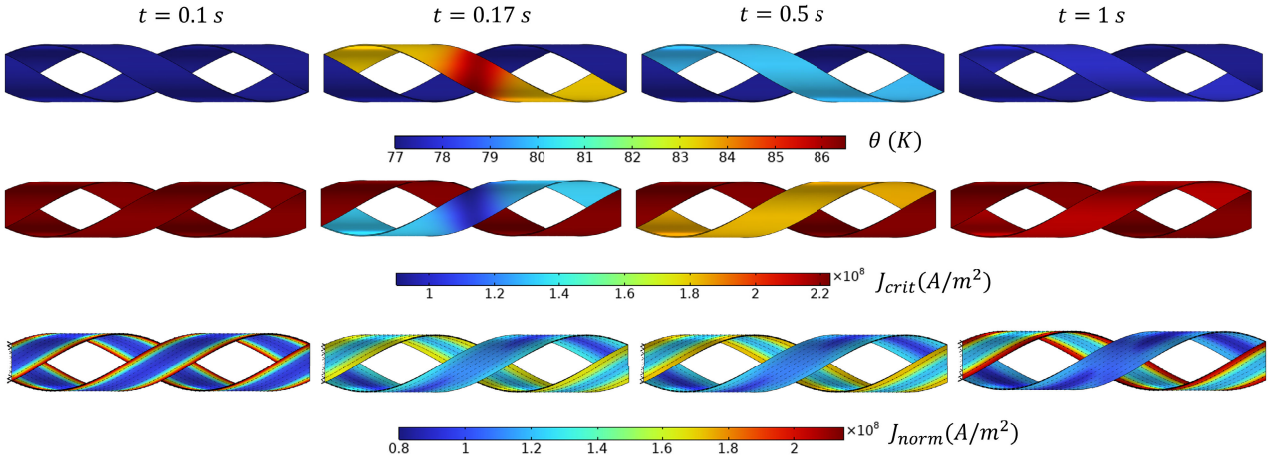

FIGURE 13. Temperature, critical current density and current density norm maps at different timesteps in the 2-tapes CORC® computed in $T - A$ model.

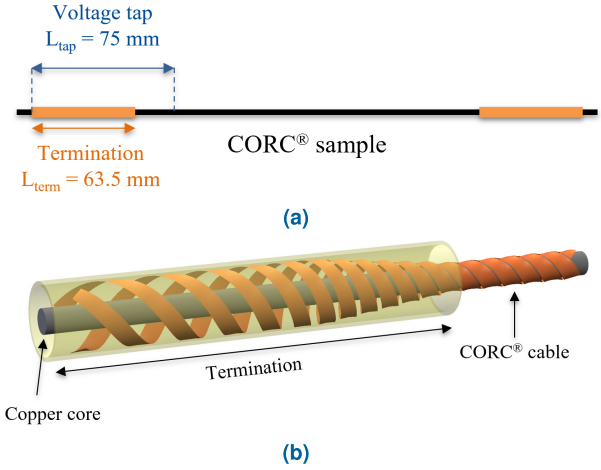

FIGURE 14. (a) Experimental set up. (b) Detail of CORC® cable within the termination.

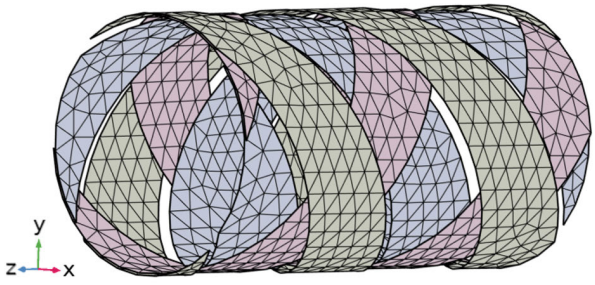

FIGURE 15. Illustration of the 3D meshed CORC® cable with larger inner diameter used for the solution in COMSOL.

manufacturer, the expected nominal critical current for a straight non-twisted cable and without taking into account of the self-field effects, is $I_c = 378$ A [15]. From experience [private communication, 2022], however, it was observed that the nominal of $I_c = 378$ A normally is reduced by 20−30% due to the self-field effects generated by the twisting of the CORC® and to the presence of the terminations, leading to an expected I_c value that lies withing the range of $260 - 300$ A. The measured I_c for the straight CORC® is indeed 262.5 A, evaluated at the average electric field of 100 μV/m. The termination is 63.5 mm long and the voltage taps is set at 75 mm from the termination, see Fig. 14a. Further reduction of I_c occurs in the terminations, since the tapes are spreading out and the inner radius is larger (see Fig. 14b). At the terminations, self-field effects is more pronounced with respect to the center of the CORC® wire with the nominal radius and resistive effects may occur.

2) SIMULATION SET-UP

The simulations aim at reproducing the $V - I$ curve experiments carried out in a bath of liquid nitrogen at 77 K in straight conditions. The current is ramped up and then wait for the stationary conditions. The tape critical current will decrease due to winding process. The degradation of 25% ($\psi = 0.75$) has been evaluated from Fig. 2 and the maximum strain $\approx -0.7\%$ from Eq. (5) (in good agreement with what has been computed and measured in [17]), so that the I_{c0} for each tape wounded on the CORC® is 63.75 A. Three sets of simulation have been carried out: first, a pitch of the main CORC® wire with the nominal winding radius at 77 K; then, a pitch of CORC® wire within the termination at 77 K, to account for the tapes spreading out and, finally, the last geometry at 80 K to consider a possible Joule effect in the termination.

3) MESH

The 3D air domain has been discretized with an unstructured tetrahedral mesh (about 25000 tetrahedra) and the 2D CORC® tape surfaces with unstructured triangular mesh (about 3800 triangles), see Fig. 15.

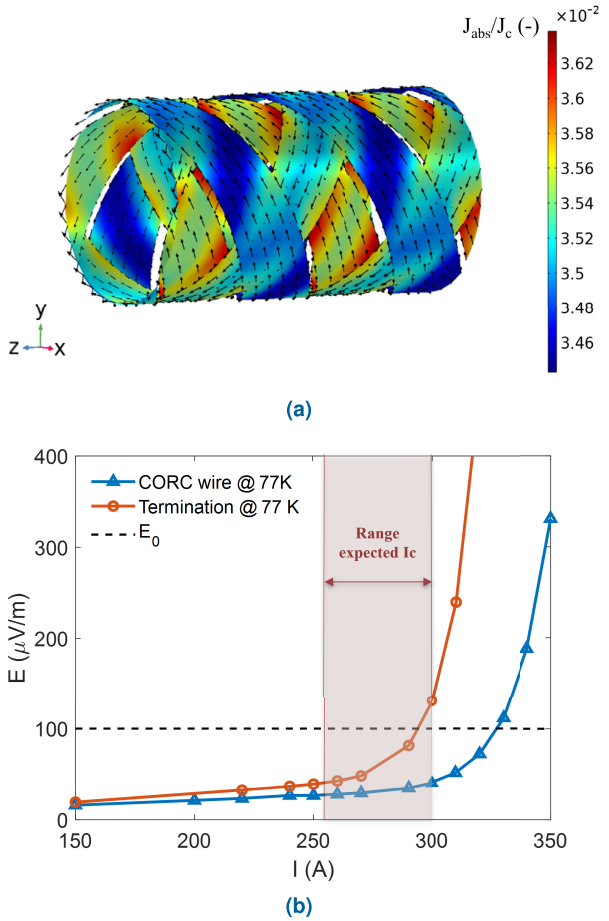

FIGURE 16. 6-tape CORC® cable in self field: (a) Magnitude of the current density norm J_{abs} over critical current density J_c when steady-state is reached: non-homogeneous current distribution among tapes; (b) Computed $E - I$ curves comparison: blue CORC® wire and red termination both at 77 K.

4) RESULTS

In Fig. 16a, the norm of the current density distribution J_{abs} over the critical current density J_c in self-field is shown. The input current is 200 A (each tape experiences $\approx$ 0.5 I_{c0}), so we are fully in the superconductive state. Even though the temperature is uniform at 77 K, it is possible to notice that the current distribution is not uniform: this is due to the non-uniform self-induced magnetic field by the cable in different tapes. This result is demonstrating that the model is able to properly calculate the current redistribution among tapes, not just for a thermal perturbation, but even for a magnetic disturbance. The magnetic field, of the order of few mT, is higher in the outermost layer and lower in the innermost layer since the former is subject to the magnetic field induced by the internal layer. Moreover, the magnetic field is stronger where tapes overlap. This reduces locally the critical current and thus increases the resistivity, with a consequent current redistribution and non-uniformity. That is guaranteed by the novel boundary condition adopted in this study. In Fig. 16b the electric field E versus the current I curves of the main CORC® wire is compared with the $E - I$ curve of CORC® within the termination (wire with

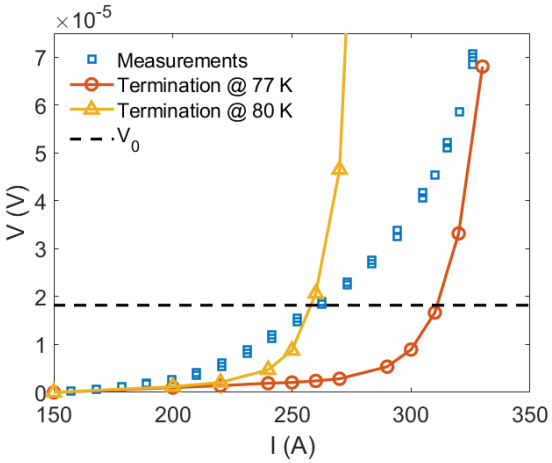

FIGURE 17. $V - I$ curves comparison: measurements (blue square), computations within the termination at 77 K (red solid line), and computations within the termination at 80 K (yellow solid line). V_0 is the voltage criterion.

the larger winding radius) at 77 K. The I_c computed for the termination is well in line with the expectations from the manufacturers (292 A). While the $E - I$ curve, computed for the CORC® with its original radius, gave back a much higher critical current than expected (327 A). The critical current in the termination further reduces if a local heating is considered due to Joule effect in the termination - here the effect has been reproduced in a simplified way assuming a temperature of 80 K as boundary condition for the simulation. The value of the experimental voltage is reported in Fig. 17 as a function of the current, and compared with the value computed from the simulations. The computed voltage $V_{computed}$ is given by the sum of an average voltage drops in the termination and in the main cable as follows:

$$V_{computed} = \int_{L_{tap}} \mathbf{E}_{main} \cdot \mathrm{d}\mathbf{l} + \int_{L_{term}} \mathbf{E}_{term} \cdot \mathrm{d}\mathbf{l} \qquad (22)$$

where $\mathbf{E}_{main}$ is the electric field computed for a pitch of CORC® wounded according to the nominal former diameter, L_{tap} corresponds to the length at which the tap is located (75 mm), $\mathbf{E}_{term}$ is the electric field computed for CORC® within the termination and L_{term} is the termination length (63.5 mm), see Fig. 14a. The experimental critical current in Fig. 17 (262.5 A) is in the expected range, but lower than the one computed with the termination at 77 K. When the termination is assumed at 80 K, which seems compatible with the temperature increase at the termination, the computed I_c is closer to the experimental value (258 A). Moreover, the discrepancy may be not only due to a higher temperature within the termination, but also a possible variation of the conductor properties: it might be possible that some tapes could be affected by defects reflecting in a smaller critical current also in the CORC® wire.

V. CONCLUSION

A multi-physics numerical model for the characterization of the critical current of HTS tapes, based on the hybrid

$T - A$ formulation coupled with the heat equation has been proposed here capable to reproduce the $V - I$ curve of a straight CORC® cable. The model has been subject to benchmark and validations among different formulations and to compare the experimental measurements, whenever possible.

Specifically, the single tape 3D model has been verified and benchmarked for different applied field with a 2D magnetostatic model for the I_c prediction has been, proving the capability of the model to deal with the strong non-linearity of the problem. The model has been extended to a CORC® cable geometry: the minimum computational domain, a single pitch of the cable, has been simulated to reduce the computational cost. Edge-effects have been avoided by imposing of periodic boundary conditions. The current distribution and redistribution among tapes is computed self-consistently though the novel boundary condition. This capability has been proved though a benchmark with a 3D model based on $H-$formulation, in which one of the tapes has perturbed with a heat pulse. The comparison showed a good agreement with the reference. Finally, a 6-tape CORC® model have been used to computed the $V-I$ curves, validated through experimental data. While the single tape showed a good agreement with measurements, the $V - I$ curve for a 3-layers (6-tapes) straight CORC® cable, pointed out that the measured I_c value can be explained accounting for the termination geometry and possible Joule heating leading to an increase in the cable temperature and the possible presence of defects in the tape, not considered in the numerical model. The model still needs more validation for different cable layout configurations and scenarios. Nonetheless, the implemented model allows the prediction of transport performance and behavior of CORC® cables and it could help for improving the termination development.

APPENDIX

This appendix is devoted to a deeper explanation of the novel boundary condition for the $T - A$ formulation implemented in COMSOL Multiphysics®.

To impose a uniform and equal T to subsequent edges (Fig. 18), we utilized the *General Extrusion* feature *Component -> Definition -> General Extrusion*.

The *General Extrusion* operator allows to map a variable from a *source* entity to a *destination* one and allowing operations such as translating, rotating, mirroring or scaling the mapped variables. In this case, the variable of interest is the current vector potential T and we want to force them to be the same via a rotation.

To map the T from the red edge in Fig. 18 to the blue one:

$$genext1 = \begin{cases} x = x\cos(\alpha) - y\sin(\alpha) \\ y = x\sin(\alpha) + y\cos(\alpha) \end{cases} \tag{23}$$

where α is the angle between the two edges, see Fig. 18. To map the T from the blue edge to the red one, the angle has to be considered in the opposite direction as in (24).

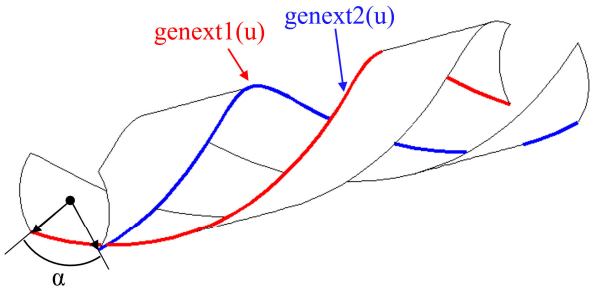

FIGURE 18. Representation of the novel boundary condition application in COMSOL [40].

$$genext2 = \begin{cases} x = x\cos(-\alpha) - y\sin(-\alpha) \\ y = x\sin(-\alpha) + y\cos(-\alpha) \end{cases} \tag{24}$$

Then, the mapped T, express as $genext1(u)$ (where u is the name of variable in COMSOL), is imposed to the blue edge as a Dirichlet boundary condition, and viceversa for $genext2(u)$. The same method has been applied for the imposition of the periodic boundary conditions.

ACKNOWLEDGMENT

The authors would like to thank C. Messe from LBNL for helpful discussions about numerical modeling, also would like to thank Tengming Shen from LBNL for his help and support, also would like to thank D. Van der Laan and J. Weiss from Advanced Conductor Technologies LLC for sharing expertise on CORC® cable behavior, also would like to thank M. Zhang and W. Yuan from the Applied Superconductivity Laboratory, University of Strathclyde, for sharing COMSOL model, and also would like to thank H. Yong from Lanzhou University for consultancy about TA formulation.

REFERENCES

[1] D. I. Meyer and R. Flasck, "A new configuration for a dipole magnet for use in high energy physics applications," *Nucl. Instrum. Methods*, vol. 80, no. 2, pp. 339–341, Apr. 1970.

[2] G. Ambrosio, "Nb3Sn high field magnets for the high luminosity LHC upgrade project," *IEEE Trans. Appl. Supercond.*, vol. 25, no. 3, pp. 1–7, Jun. 2015.

[3] L. G. Fajardo, T. Shen, X. Wang, C. Myers, D. Arbelaez, E. Bosque, L. Brouwer, S. Caspi, L. English, S. Gourlay, A. Hafalia, M. Martchevskii, I. Pong, and S. Prestemon, "First demonstration of high current canted-cosine-theta coils with Bi-2212 Rutherford cables," *Superconductor Sci. Technol.*, vol. 34, no. 2, Feb. 2021, Art. no. 024001.

[4] J. van Nugteren, G. Kirby, J. Murtomäki, G. DeRijk, L. Rossi, and A. Stenvall, "Toward REBCO 20 T+ dipoles for accelerators," *IEEE Trans. Appl. Supercond.*, vol. 28, no. 4, pp. 1–9, Jun. 2018.

[5] S. Caspi, F. Borgnolutti, L. Brouwer, D. Cheng, D. R. Dietderich, H. Felice, A. Godeke, R. Hafalia, M. Martchevskii, S. Prestemon, E. Rochepault, C. Swenson, and X. Wang, "Canted–Cosine–Theta magnet (CCT)—A concept for high field accelerator magnets," *IEEE Trans. Appl. Supercond.*, vol. 24, no. 3, pp. 1–4, Jun. 2014.

[6] B. N. Sorbom, "ARC: A compact, high-field, fusion nuclear science facility and demonstration power plant with demountable magnets," *Fusion Eng. Des.*, vol. 100, p. 28, Nov. 2015.

[7] M. Bonura and C. Senatore, "High-field thermal transport properties of REBCO coated conductors," *Superconductor Sci. Technol.*, vol. 28, no. 2, Feb. 2015, Art. no. 025001.
[8] A. K. Jha and K. Matsumoto, "Superconductive REBCO thin films and their nanocomposites: The role of rare-earth oxides in promoting sustainable energy," *Frontiers Phys.*, vol. 7, p. 82, Jun. 2019.
[9] H. Piekarz, S. Hays, J. Blowers, B. Claypool, and V. Shiltsev, "Record fast-cycling accelerator magnet based on HTS conductor," *Nucl. Instrum. Methods Phys. Res. A, Accel. Spectrom. Detect. Assoc. Equip.*, vol. 943, Nov. 2019, Art. no. 162490.
[10] D. C. Larbalestier, J. Jiang, U. P. Trociewitz, F. Kametani, C. Scheuerlein, M. Dalban-Canassy, M. Matras, P. Chen, N. C. Craig, P. J. Lee, and E. E. Hellstrom, "Isotropic round-wire multifilament cuprate superconductor for generation of magnetic fields above 30 T," *Nature Mater.*, vol. 13, no. 4, pp. 375–381, Apr. 2014.
[11] D. C. van der Laan, "$YBa_2Cu_3O_{7-\delta}$ coated conductor cabling for low AC-loss and high-field magnet applications," *Supercond. Sci. Technol.*, vol. 22, no. 6, Jun. 2009, Art. no. 065013.
[12] J. D. Weiss, T. Mulder, H. J. T. Kate, and D. C. van der Laan, "Introduction of CORC® wires: Highly flexible, round high-temperature superconducting wires for magnet and power transmission applications," *Supercond. Sci. Technol.*, vol. 30, no. 1, Jan. 2017, Art. no. 014002.
[13] Z. Guo, J. Qin, R. Lubkemann, K. Wang, H. Jin, G. Xiao, J. Li, C. Zhou, and A. Nijhuis, "AC loss and contact resistance in highly flexible REBCO cable for fusion applications," *Superconductivity*, vol. 2, Jun. 2022, Art. no. 100013.
[14] G. Xiao, H. Jin, C. Zhou, H. Ma, D. Wang, F. Liu, H. Liu, A. Nijhuis, and A. Devred, "Performance of highly flexible sub-cable for REBCO cable-in-conduit conductor at 5.8 T applied field," *Superconductivity*, vol. 3, Sep. 2022, Art. no. 100023.
[15] D. C. van der Laan, J. D. Weiss, and D. M. McRae, "Status of CORC® cables and wires for use in high-field magnets and power systems a decade after their introduction," *Supercond. Sci. Technol.*, vol. 32, no. 3, Mar. 2019, Art. no. 033001.
[16] P. Gao, J. Mao, J. Chen, X. Wang, and Y. Zhou, "Electromechanical degradation of REBCO coated conductor tapes under combined tension and torsion loading," *Int. J. Mech. Sci.*, vol. 223, Jun. 2022, Art. no. 107314.
[17] F. Pierro, Z. Zhao, C. M. Owen, C. Colcord, L. Chiesa, H. C. Higley, X. Wang, and S. O. Prestemon, "Finite-element analysis of the strain distribution due to bending in a REBCO coated conductor for canted cosine theta dipole magnet applications," *IEEE Trans. Appl. Supercond.*, vol. 29, no. 5, pp. 1–5, Aug. 2019.
[18] J. Yan, K. Wang, Y. Gao, Y. Zhou, and A. Nijhuis, "Investigating the effect of transverse compressive loads on the electromagnetic performance of superconducting CORC® cables," *Supercond. Sci. Technol.*, vol. 35, no. 11, Nov. 2022, Art. no. 115006.
[19] V. A. Anvar, K. Ilin, K. A. Yagotintsev, B. Monachan, K. B. Ashok, B. A. Kortman, B. Pellen, T. J. Haugan, J. D. Weiss, D. C. van der Laan, R. J. Thomas, M. J. Prakash, M. S. A. Hossain, and A. Nijhuis, "Bending of CORC® cables and wires: Finite element parametric study and experimental validation," *Supercond. Sci. Technol.*, vol. 31, no. 11, Nov. 2018, Art. no. 115006.
[20] R. Hu, Y. Yuan, Y. Chen, W. Li, H. Ye, J. Sheng, Y. Zhao, and Z. Jin, "Numerical study on mechanical properties of conductors on round core cables," *IEEE Trans. Appl. Supercond.*, vol. 31, no. 5, pp. 1–5, Aug. 2021.
[21] X. Li, Y. Xu, L. Ren, and Y. Tang, "Improved mechanical models and ic estimation for the whole life cycle of high temperature superconducting coated conductors," *Compos. Struct.*, vol. 298, Oct. 2022, Art. no. 116000.
[22] K. Wang, Y. W. Gao, V. A. Anvar, K. Radcliff, J. D. Weiss, D. C. van der Laan, Y. H. Zhou, and A. Nijhuis, "Prediction of strain, interlayer interaction and critical current in CORC® wires under axial strain by T–A modeling," *Supercond. Sci. Technol.*, vol. 35, no. 10, Oct. 2022, Art. no. 105012.
[23] R. Teyber, M. Marchevsky, A. C. A. Martinez, S. Prestemon, J. Weiss, and D. van der Laan, "Numerical investigation of current distributions around defects in high temperature superconducting CORC® cables," *Supercond. Sci. Technol.*, vol. 35, no. 9, Sep. 2022, Art. no. 094008.
[24] X. Li, L. Ren, Y. Xu, J. Shi, X. Chen, G. Chen, Y. Tang, and J. Li, "Calculation of CORC cable loss using a coupled electromagnetic-thermal T–A formulation model," *IEEE Trans. Appl. Supercond.*, vol. 31, no. 4, pp. 1–7, Jun. 2021.
[25] X. Li, L. Ren, Y. Xu, J. Long, J. Shi, G. Chen, Y. Yue, and Y. Tang, "Study on the influence of thermal and magnetic field on CORC cable properties by a 2D model," *IEEE Trans. Appl. Supercond.*, vol. 31, no. 8, pp. 1–5, Nov. 2021.
[26] S. Wang, H. Yong, and Y. Zhou, "Calculations of the AC losses in superconducting cables and coils: Neumann boundary conditions of the T–A formulation," *Supercond. Sci. Technol.*, vol. 35, no. 6, Jun. 2022, Art. no. 065013.
[27] B. Shen et al., "A simplified model of the field dependence for HTS conductor on round core (CORC) cables," *IEEE Trans. Appl. Supercond.*, vol. 31, no. 8, pp. 1–5, Nov. 2021.
[28] B. Shen et al., "Superconducting conductor on round core (CORC) cables: 2D or 3D modeling?" *IEEE Trans. Appl. Supercond.*, vol. 31, no. 8, pp. 1–5, Nov. 2021.
[29] Z. Zhu, "Advanced 3D and 2D modelling of HTS CORC cable based on the T–A formulation for the propulsion system of hybrid-electric aircraft," Ph.D. dissertation, Dept. Electron. Elect. Eng., Univ. Bath, Bath, U.K., 2020.
[30] R. Brambilla, F. Grilli, and L. Martini, "Development of an edge-element model for AC loss computation of high-temperature superconductors," *Supercond. Sci. Technol.*, vol. 20, no. 1, pp. 16–24, Jan. 2007.
[31] Z. Hong, A. M. Campbell, and T. A. Coombs, "Numerical solution of critical state in superconductivity by finite element software," *Supercond. Sci. Technol.*, vol. 19, no. 12, pp. 1246–1252, Dec. 2006.
[32] M. Tian, J. Yang, B. Shen, Y. Öztürk, J. Ma, C. Li, J. Hu, H. Wei, J. Li, and T. Coombs, "Analysis on the effect of superconductor layer thickness on the AC loss of conductor on round core (CORC) cables," *IEEE Trans. Appl. Supercond.*, vol. 31, no. 8, pp. 1–4, Nov. 2021.
[33] M. U. Fareed, M. Kapolka, B. C. Robert, M. Clegg, and H. S. Ruiz, "3D modelling and validation of the optimal pitch in commercial CORC cables," *IOP Conf. Ser., Mater. Sci. Eng.*, vol. 1241, no. 1, May 2022, Art. no. 012030.
[34] M. U. Fareed, M. Kapolka, B. C. Robert, M. Clegg, and H. S. Ruiz, "3D FEM modeling of CORC commercial cables with bean's like magnetization currents and its AC-losses behavior," *IEEE Trans. Appl. Supercond.*, vol. 32, no. 4, pp. 1–5, Jun. 2022.
[35] H. Zhang, M. Zhang, and W. Yuan, "An efficient 3D finite element method model based on the T–A formulation for superconducting coated conductors," *Supercond. Sci. Technol.*, vol. 30, no. 2, Feb. 2017, Art. no. 024005.
[36] Y. Wang, Y. Wang, D. Wei, T. Guo, Y. Meng, J. Wang, and C. Kan, "AC losses of a like-CORC conductor using accelerated 3D T–A model," *Phys. C, Supercond. Appl.*, vol. 579, Dec. 2020, Art. no. 1353770.
[37] Y. Wang, M. Zhang, F. Grilli, Z. Zhu, and W. Yuan, "Study of the magnetization loss of CORC® cables using a 3D T–A formulation," *Supercond. Sci. Technol.*, vol. 32, no. 2, Feb. 2019, Art. no. 025003.
[38] Z. Zhu, Y. Wang, D. Xing, X. Pei, M. Zhang, and W. Yuan, "Quench of a single-layer ReBCO CORC cable with non-uniform terminal contact resistance," *IEEE Trans. Appl. Supercond.*, vol. 29, no. 5, pp. 1–5, Aug. 2019.
[39] Y. Wang, J. Zheng, Z. Zhu, M. Zhang, and W. Yuan, "Quench behavior of high-temperature superconductor $(RE)Ba_2Cu_3O_x$ CORC cable," *J. Phys. D, Appl. Phys.*, vol. 52, no. 34, Aug. 2019, Art. no. 345303.
[40] *COMSOL Multiphysics Reference Manual*, COMSOL Inc., Burlington, MA, USA, 2022.
[41] *Home Page | SuperPower*, SuperPower Inc., Glenville, NY, USA, 2022.
[42] J. Fleiter and A. Ballarino, "In-field electrical resistance at 4.2 k of REBCO splices," *IEEE Trans. Appl. Supercond.*, vol. 27, no. 4, pp. 1–5, Jun. 2017.
[43] M. Casali, "Experimental analysis and numerical simulation of quench in superconducting HTS tapes and coils," Ph.D. dissertation, Dept. Electr., Electron. Inf. Eng. 'Guglielmo', Univ. Bologna, Bologna, Italy, 2014.
[44] B. C. Robert, M. U. Fareed, and H. S. Ruiz, "How to choose the superconducting material law for the modelling of 2G-HTS coils," *Materials*, vol. 12, no. 17, p. 2679, Aug. 2019.
[45] F. Grilli, F. Sirois, V. M. R. Zermeno, and M. Vojenciak, "Self-consistent modeling of the I_c of HTS devices: How accurate do models really need to be?" *IEEE Trans. Appl. Supercond.*, vol. 24, no. 6, pp. 1–8, Dec. 2014.
[46] X. Wang, D. R. Dietderich, A. Godeke, S. A. Gourlay, M. Marchevsky, S. O. Prestemon, and G. L. Sabbi, "Performance correlation between $YBa_2Cu_3O_{7-\delta}$ coils and short samples for coil technology development," *Supercond. Sci. Technol.*, vol. 29, no. 6, Jun. 2016, Art. no. 065007.
[47] F. Gömöry and B. Klinčok, "Self-field critical current of a conductor with an elliptical cross-section," *Supercond. Sci. Technol.*, vol. 19, no. 8, pp. 732–737, May 2006.
[48] T. L. Bergman, *Introduction to Heat Transfer*, 6th ed. Hoboken, NJ, USA: Wiley, 2011.

[49] S. Sparacio, S. Viarengo, F. Ledda, D. Torsello, N. Riva, Z. Hartwig, L. Savoldi, and F. Laviano, "Analysis of thermal effects of plasma operation on HTS-basted TF-coil conductors," in *Proc. EUCAS*, Sep. 2023.
[50] Y. Yan, T. Qu, and F. Grilli, "Numerical modeling of AC loss in HTS coated conductors and Roebel cable using T–A formulation and comparison with H formulation," *IEEE Access*, vol. 9, pp. 49649–49659, 2021.
[51] M. Ainslie, F. Grilli, L. Quéval, E. Pardo, F. Perez-Mendez, R. Mataira, A. Morandi, A. Ghabeli, C. Bumby, and R. Brambilla, "A new benchmark problem for electromagnetic modelling of superconductors: The high-T_c superconducting dynamo," *Supercond. Sci. Technol.*, vol. 33, no. 10, Oct. 2020, Art. no. 105009.
[52] E. Berrospe-Juarez, V. M. R. Zermeño, F. Trillaud, and F. Grilli, "Real-time simulation of large-scale HTS systems: Multi-scale and homogeneous models using the T–A formulation," *Supercond. Sci. Technol.*, vol. 32, no. 6, Jun. 2019, Art. no. 065003.
[53] J. Stern, J. Swanson, T. Bogdanof, M. Krutulis, J. Weiss, D. van der Laan, X. Wang, and L. Chiesa, "Developing a vacuum pressure impregnation procedure for CORC wires," *IEEE Trans. Appl. Supercond.*, vol. 32, no. 6, pp. 1–4, Sep. 2022.

SOFIA VIARENGO (Graduate Student Member, IEEE) received the M.Sc. degree in energy and nuclear engineering from Politecnico di Torino, Turin, Italy, in 2020. She is currently pursuing the dual Ph.D. degree in energetics with Politecnico di Torino and the Lawrence Berkeley National Laboratory, Berkeley, CA, USA. During the Ph.D. degree, she has been dedicated to the development of electric model for electromagnetic transients in forced-flow superconducting cables for fusion and power applications. She became familiar with CORC® -like cable for accelerator applications with the Lawrence Berkeley National Laboratory. Her research interests include the development of multiphisycs numerical models for normal and off-normal operations for high temperature superconducting component, from thermal and electromagnetic point of view.

LUCAS BROUWER received the Ph.D. degree in nuclear engineering from the University of California at Berkeley, Berkeley, in 2015. His Ph.D. thesis focused on the canted-cosine theta (CCT) accelerator magnet design. He is currently a Research Scientist with the Accelerator Technology and Applied Physics Division, Lawrence Berkeley National Laboratory. His current research interests include the engineering design and test of 10 T + Nb_3Sn dipole magnets for high energy physics, large momentum acceptance gantry magnets for proton therapy, and ultra-stable superconducting magnets for electron microscopy.

PAOLO FERRACIN (Senior Member, IEEE) received the M.Sc. degree (cum laude) in nuclear engineering and the Ph.D. degree in energetics, in 1998 and 2002, respectively. He joined the CERN Main Magnet and Superconductors Group as a Ph.D. Student to work on the mechanics and magnetics of the main superconducting dipole magnets for the large hadron collider (LHC). In May 2002, he started working with the Lawrence Berkeley National Laboratory (LBNL), Superconducting Magnet Program (SMP), as a Physicist Postdoctoral Fellow and then as a Staff Scientist on the development of Nb_3Sn dipoles and quadrupoles for the next generation particle accelerators. In 2011, he rejoined the CERN Magnets, Superconductors and Cryostats Group as a Staff working on Nb_3Sn superconducting magnets, and in 2012, he started leading the development of MQXFB, the Nb_3Sn low-β quadrupole magnet for the High Luminosity LHC (HL-LHC) Project. Since February 2020, he has been the SMP Program Deputy with LBNL.

FABIO FRESCHI (Senior Member, IEEE) received the M.Sc. (summa cum laude) and Ph.D. degrees in electrical engineering from Politecnico di Torino, in 2002 and 2006, respectively. In 2006, he was a Visiting Researcher with the Technical University of Graz, Graz, Austria. He was appointed as an Adjunct Senior Fellow with The University of Queensland, Australia, from 2014 to 2020. He is currently a Full Professor in fundamentals of electrical engineering with Politecnico di Torino. His research and scientific interests include the numerical modeling and computation of electromagnetic and coupled fields using differential, integral, and hybrid techniques. He has coauthored more than 150 journals and conference papers in these fields. He was a recipient of several international awards issued by IEEE. Since 2022, he has been included in the World's 2% Top Scientist list prepared by Stanford University and Elsevier. He is an Associate Editor of IEEE TRANSACTIONS ON INDUSTRY APPLICATIONS, and he serves as referee of many international journals in the field of numerical electromagnetics, optimization, and operational research.

NICOLO' RIVA received the M.Sc. degree (summa cum laude) in physics from the University of Milano, in 2016, and the Ph.D. degree in electrical engineering from Ecole Polytechnique Federale de Lausanne (EPFL), in 2020. He has specialized experience in FEM simulations having worked on aspects, such as quench protection for the MQXF quadrupole (QLAS—LASA Milano) and superconducting devices for space applications (INFN Genova and OHB-Italia). His Ph.D. research was focused on combining FEM modeling for HTS with experimental measurements for the characterization of the overcritical current resistivity of REBCO-coated conductors. He is currently a Postdoctoral Researcher with the Plasma Science and Fusion Center, Massachusetts Institute of Technology (PSFC-MIT). He also collaborates with Type One Energy (T1E) and Commonwealth Fusion Systems (CFS) on magnets for fusion (e.g., SPARC and STARBLAZeR), evaluating the risks in the use of REBCO HTS for fusion magnets using numerical simulations and experiments.

LAURA SAVOLDI (Member, IEEE) received the M.Sc. degree (cum laude) in nuclear engineering and the Ph.D. degree in energetics from Politecnico di Torino, Turin, Italy, in 1997 and 2001, respectively. She is currently a Full Professor in nuclear plants with Politecnico di Torino. Her research interests include the development, validation, and application of computational tools for the analysis of thermal-hydraulic transients in advanced heat transfer problems, including superconducting magnets. In this frame, she developed the 4C code for the analysis of thermal-hydraulic transients in superconducting cables, coils, and related cryogenic circuits. She has coauthored more than 200 papers published in international journals and proceedings of international conferences. She serves as a referee for several international journals and conferences of her field of research, among which IEEE TRANSACTIONS ON APPLIED SUPERCONDUCTIVITY and IEEE TRANSACTIONS ON PLASMA SCIENCE.

XIAORONG WANG (Senior Member, IEEE) received the Ph.D. degree in electrical engineering from Florida State University, in 2008, on the quench behavior of ReBCO conductors. Together with colleagues and collaborators, he is a part of the U.S. Magnet Development Program that develops ReBCO accelerator magnet technology. He is currently a Scientist with the Accelerator Technology and Applied Physics Division, Lawrence Berkeley National Laboratory.

Open Access funding provided by 'Politecnico di Torino' within the CRUI CARE Agreement